IEEE Access
Multidisciplinary | Rapid Review | Open Access Journal

Received July 15, 2019, accepted July 21, 2019, date of publication July 29, 2019, date of current version August 14, 2019.

Digital Object Identifier 10.1109/ACCESS.2019.2931796

Vertical Stabilization Control for Trimaran Based on Resultant Force and Moment Distribution

ZHILIN LIU, LINHE ZHENG, GUOSHENG LI, AND BOWEN ZENG
College of Automation, Harbin Engineering University, Harbin 150001, China

Corresponding author: Linhe Zheng (zlh@hrbeu.edu.cn)

This work was supported by the National Natural Science Foundation of China under Grant 51379044.

ABSTRACT The vertical movement of a trimaran caused by external disturbances during sailing, may lead to seasickness of the passengers and damage of the equipment onboard. Based on computational fluid dynamics (CFD) calculations, the hydrodynamic coefficients are obtained and a mathematical model of the trimaran is established, and with experiments of trimaran sailing in water tanks, the hydrodynamic coefficients solved by CFD are verified. Then, the T-foil and flap are designed, and the lift force and moment are solved by CFD. Next, the slope of the force of different attack angles on the T-foil and flap is obtained by the polynomial fitting. Finally, the trimaran vertical stabilization proportion and derivative (PD) controller, based on the sigmoid function, is designed with a new method of the resultant force and moment for a dynamic decoupling T-foil and flap. Through the simulation of trimaran movements systems with active T-foil and flap, the PD parameters are obtained. Then, the effect of the controller on trimaran vertical stabilization is verified by the experiments in the water tanks.

INDEX TERMS Trimaran vertical stabilization control, T-foil and flap dynamic decoupling, numerical simulation, resultant force and moment distribution.

I. INTRODUCTION

A trimaran is a kind of multihull ship and it can produce movement when sailing in the sea. When compared to monohulled ship, the heave and pitch of a multihull ship are both more violent. The large pitch and heave can cause the seasickness of the crew and damage to the trimaran's equipment [1]. Reducing the vertical movement of the trimaran is a cause of great concern among engineers and technicians in different countries. The most commonly used method is to install appendages on the bottom of the ship. Many appendages for ship stability have been used [2]. For example, [3] designed a bilge keel to reduce the roll motion, [4] used fin and rudders to alleviate the roll motion, T-foil and tabs are used in the ride control system and can reduce the heave and pitch effects [5]. In [6], T-foil and flaps are installed to the ship together to reduce the ship's vertical acceleration. The appendages are divided into passive and active appendage. Passive appendages have vertical stabilization effects, but the force and moment by the appendage is limited. Reference [7] gives a comparison of a trimaran with active control T-foil and passive T-foil, the result showed that the actively controlled T-foil can improve the effect of heave and pitch by approximately 20% more than passive T-foil. In [8] and [9], a fast ferry installed with a T-foil and flaps together with the active control, the MSI (motion sickness incidence) and WVA (worst vertical acceleration) show obvious improvements.

The active control algorithm, references [10], [11], show that the fast ferry with a T-foil and flaps was effective in reducing the vertical movement using WVA as a PD control index. Multivariable classic control was used to decrease the MSI of a high speed ferry [12]. de la Cruz [8] used a multivariable robust controller, and a fuzzy control is used in [9]. The results of [9], verified the effectiveness of the advanced algorithm and could be used in an actual marine environment. Sliding mode control [13] and model predictive control [14] are also used in the research of ship motion stabilization. An optimal PD controller based on the genetic algorithm is presented [10], and the research obtained satisfactory results. Reference [15] used a linear quadratic regulator for wave piercing catamarans motion control, and reference [16] showed an intelligent control based on PSO (Particle swarm optimization) for a ship roll motion. Luo *et al.* [17] presented an adaptive robust fin controller based on a feedforward neural network. These advanced methods have excellent results in simulation, but they are hard to accomplish in

The associate editor coordinating the review of this manuscript and approving it for publication was Jun Shen.

actual engineering. The decoupling PD control presented in [10] was successfully applied in actual engineering. However, it needed to decouple the control input of the T-foil and flap, and after decoupling the difference equation order was too high. Then, a simple and easy method is presented in this article, and the PD controller based on the sigmoid function is used to reduce the heave and pitch motions.

Simulations of trimaran sailing in different speeds and sea states is necessary for controller design. The simulations are based on mathematical models of the trimaran, the actuators, and the waves. The parameters of the mathematical model need to be identified. In recent years, CFD has been widely used in experiments, such as [18]–[20]. Reference [21] used CFD to predict the roll added mass moment of inertia of a ship, and the numerical simulation results are consistent with the experimental results. Wang *et al.* [22] and Shen *et al.* [23] used overset grid technology for the trimaran's movement, and the technology could handle large amplitude motion well. We also used overset grid in this paper. After the trimaran hydrodynamic coefficients are calculated, the trimaran movement equation is obtained. Reference [24] showed the computational process of wave to heave and pitch, the computational process divided into wave energy spectrum, wave force and moment, and ship movement equation. In this paper, a wave energy spectrum is selected by the ITTC (International Towing Tank Conference) two parameter spectra [25], PSO is used to best fit the data point and adds the constraints to make the denominator a negative root.

The paper is organized as follows. Section 2 presents the mathematical model of the trimaran heave and pitch as well as the computational methods of the hydrodynamic coefficients of trimaran. Section 3 gives the dimension, shape and installation position of the actuator to the trimaran, simulates the fixed actuator for the heave and pitch and compares this to the trimaran without the actuator. In Section 4, details of the controller design are presented. In Section 5, experimental results are presented and reported. Finally, Section 6 concludes the present work.

II. MATHEMATICAL MODEL OF THE TRIMARAN EQUATION

To solve the control problem of the trimaran vertical stabilization, this paper adopts the method of installing an active T-foil and flap. A trimaran movement mathematical model is established. Reference [26] gives us a nonlinear 6-DOF motion system of equations, and the heave and pitch equations are selected as the vertical movements. For controller design, the mathematical model needs to be linearized, the following trimaran vertical equations are obtained [10]:

$$(m_t + a_{33})\ddot{x}_3 + b_{33}\dot{x}_3 + c_{33}x_3 + a_{35}\ddot{x}_5 + b_{35}\dot{x}_5 + c_{35}x_5 = F_3 \tag{1}$$

$$(I + a_{55})\ddot{x}_5 + b_{55}\dot{x}_5 + c_{55}x_5 + a_{53}\ddot{x}_3 + b_{53}\dot{x}_3 + c_{53}x_3 = M_5 \tag{2}$$

where a_{ij} are the added masses, b_{ij} are the damping coefficients, and c_{ij} are the restoring force and moment. m_t is the mass of the trimaran, I is the trimaran's moment of inertia, F_3 and M_5 are the wave force and moment amplitude, respectively.

A. TRIMARAN HYDRODYNAMIC CALCULATION

This paper adopts the CFD method to solve the hydrodynamic parameters and obtain the above parameters faster and more accurately. The trimaran studied in this paper is a 1:10 scale ship model and the trimaran's parameters are given in Table 1:

TABLE 1. Trimaran geometry parameters.

Name	Main hull	Side hulls
Length overall (m)	6.800	2.354
Length of waterline (m)	6.100	2.047
Beam (m)	1.351	0.131
Draught (m)	0.249	0.087
Depth (m)	0.517	0.362
Side hulls distance (m)	0.584	------
Center of gravity (m)	(3.04,0,0.26)	------
Displacement volume (m^3)	0.385	------
Displacement overall (kg)	509.608	------

Given the trimaran parameters above, it can be seen from the Eq. (1) and (2) that the corresponding hydrodynamic parameters need to be calculated to obtain a complete mathematical model of the trimaran. The calculated hydrodynamic parameters are generally divided into the theoretical calculation and CFD analysis. Since the research is a scale trimaran model, the wave height and period need to be scaled in the simulations and experiments. The scaling follows Froude's scaling law and the formula is as follows [27]:

$$H_{scale} = H_{actual}/P \tag{3}$$

$$T_{scale} = T_{actual}/\sqrt{P} \tag{4}$$

where H_{scale} and H_{actual} are the scaled wave height and the actual wave height, T_{scale} and T_{actual} are the period after scaling and the actual period, and finally P is the scale ratio.

The ship CFD theory is based on incompressible unsteady Reynolds-Averaged Navier-Stokes equations [23]. Based on the theory and combining the software, the hydrodynamic coefficients of trimaran under different wave directions and speeds are calculated. According to the above CFD calculation, the added mass coefficients and damping coefficients of the trimaran at the speed of 40 knots and 18 knots are obtained as shown in Fig. 1 and Fig. 2.

The restoring force and restoring moment coefficient don't change with speed and encounter frequency, and its value is shown in Table 2:

B. HYDRODYNAMIC COEFFICIENT VERIFICATION

The movement of the trimaran is shown in Fig. 3:

The main parameters of the wave are the wave height and period, under different sea conditions, the $W2F$ and $W2M$ are wave to force and moment transfer functions, which can

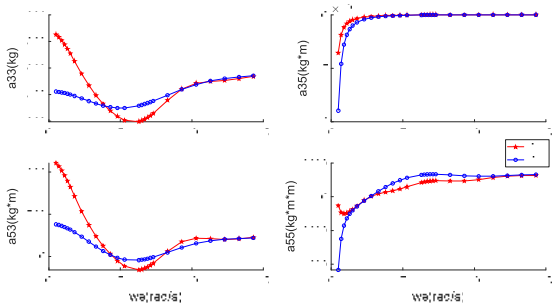

FIGURE 1. Added masses.

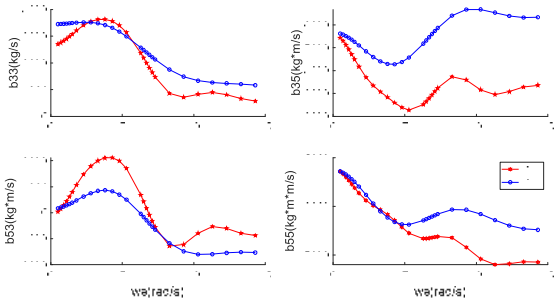

FIGURE 2. Damping coefficients.

TABLE 2. Restoring force and restoring moment.

Parameter	Value
c_{33} (N/m)	34270.0256
c_{35} (N)	4816.5574
c_{53} (N)	4816.5574
c_{55} (N/m)	100090.7347

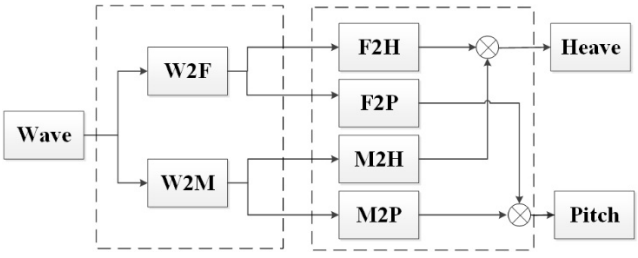

FIGURE 3. Wave to force and moment, and the force, moment to heave and pitch.

convert wave energy to wave force and moment, then, acting on the trimaran to generate heave and pitch motions. It is necessary to simulate wave force, moment, trimaran heave and pitch motions as the following reasons.

The following parts show the process of the wave to motions.

1) WAVE MODEL

This paper uses the ITTC two-parameter wave spectrum and the function $S_\zeta(\omega)$ is shown as follows:

$$S_\zeta(\omega) = (173H_S^2/T_1^4\omega^5)\exp(691/T_1^4\omega^4) \tag{5}$$

where H_S is the significant wave height and T_1 is the wave period.

2) WAVE FORCE AND MOMENT

Under the influence of the waves, the force and moment are represented as follows:

$$\begin{cases} F_{3i} = |W2Fh(j\omega_{ei})| \cdot \zeta_{ai} \cdot \sin(\omega_{ei} \cdot t + \angle W2Fh(j\omega_{ei})) \\ F_{5i} = |W2Mp(j\omega_{ei})| \cdot \zeta_{ai} \cdot \sin(\omega_{ei} \cdot t + \angle W2Mp(j\omega_{ei})) \end{cases} \tag{6}$$

where F_{3i} and F_{5i} are the wave force and moment of $i-th$ harmonic, respectively. When give a long-crested wave, in the energy concentrated band, it divides the frequency into N equal parts, and every band is $\Delta\omega$ long. Usually, N is 20∼50. Then, the wave force and moment of each harmonic are calculated, and then superimposed to obtain the wave force and moment generated by the long-wave random wave. So, the transfer functions $W2Fh(j\omega_{ei})$ and $W2Mp(j\omega_{ei})$ must be solved. We concluded by finding amplitude and phase, which are obtained by CFD simulations.

The transfer function of the wave force and moment is mainly consistent with the data points, and the method of fitting is the least square. Therefore, the form of transfer function should be given, and the wave force and moment transfer function can be expressed as the following Eq. (7) [28].

$$G(s,\theta) = \frac{B(s,\theta)}{A(s,\theta)} = \frac{b_m s^m + b_{m-1}s^{m-1} + \cdots + b_1}{s^n + a_n s^{n-1} + \cdots + a_1} \tag{7}$$

where $\theta = [b_{m+1}, b_m, b_{m-1}, \cdots, b_1, a_n, a_{n-1}, \cdots, a_1]$

In the Eq. (7) above, a_i and b_i are the transfer function coefficients, m and n are the system order. After comparing the different orders of amplitude and phase, since the order and error are the minimum, the fourth-order is chosen and PSO is used to fit the transfer function. The objective function is shown as follows:

$$J(\theta) = \sum_{i=1}^{N} |G(j\omega_i) - G(j\omega_i,\theta)|^2 \tag{8}$$

$$\hat{\theta} = \arg\min J(\theta) \tag{9}$$

where $G(j\omega_{ei})$ is the data point, $G(j\omega_{ei},\theta)$ is the fitting value of different encounter frequency.

The order is select 4 based on reference [28], and $J(\theta)$ can be expressed as follows:

$$\begin{aligned} J(\theta) &= \sum_{i=1}^{N} |G(j\omega_{ei})\exp(j\angle G(j\omega_{ei})) \\ &\quad - G(j\omega_i,\theta)\exp(j\angle G(j\omega_{ei},\theta))|^2 \\ &= \sum_{i=1}^{N} |G(j\omega_{ei})\exp(j\angle G(j\omega_{ei})) \\ &\quad - (B(j\omega_i,\theta)/A(j\omega_i,\theta))\exp(j\angle G(j\omega_{ei},\theta))|^2 \end{aligned} \tag{10}$$

where

$$B(j\omega_i,\theta)=\sqrt{(b_1-b_3\omega_i^2)^2+(b_2\omega-b_4\omega^3)^2}$$
$$A(j\omega_i,\theta)=\sqrt{(\omega^4-a_3\omega^2+a_1)^2+(a_2\omega-a_4\omega^3)^2}$$

For PSO algorithm, the particle update equations are as follows [29]:

$$V^{q+1}=wV^q+c_1r_1(P_{id}^q-X^q)+c_2r_2(P_{gd}^q-X^q) \quad (11)$$
$$X^{q+1}=X^q+V^{q+1} \quad (12)$$

where w is the inertia weight, r_1 and r_2 are random numbers in [0,1], q is the current iteration number, P_{id}^q is the optimal individual particle position, P_{gd}^q is the global optimal particle position,c_1 and c_2 are constant numbers, V is the particle's velocity, and X is the particle's position. In this fitting, $c_1=1.2$, $c_2=0.012$, $w=0.0004$, the population size is 50, and the max iterations is 10000. The result is shown in Table 3.

TABLE 3. Transfer function coefficients.

Parameters	$W2F$	$W2M$
b_1	157400	320600
b_2	14230000	14780000
b_3	15000000	14950000
b_4	-919100	-5436000
a_1	5.247	106.9
a_2	999.8	3182
a_3	551.2	978.5
a_4	137.3	132.4

With the parameters in Table 3, the transfer function can be expressed as follows:

$$W2F=\frac{919100s^3+15000000s^2+14230000s+157400}{s^4+137.3s^3+551.2s^2+999.8s+5.247} \quad (13)$$
$$W2M=\frac{-5436000s^3+14950000s^2+14780000s+3206000}{s^4+132.4s^3+978.5s^2+3182s+106.9} \quad (14)$$

Fig. 4 shows the fitted transfer function compared with the data point.

Combing Eq. (7), Eq. (8), Eq. (9), Eq. (13) and Eq. (14), the wave force and moment in SSN4 (Sea state No. 4) can be expressed in the following Fig. 5.

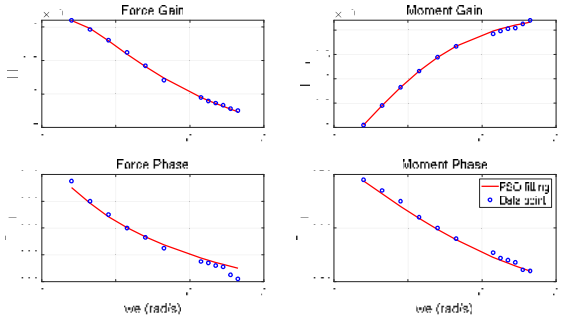

FIGURE 4. PSO fitting compared with data points.

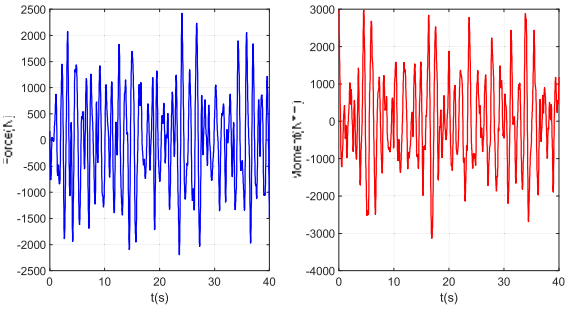

FIGURE 5. Wave force and moment under 40 knots, SSN4 on the trimaran.

3) COMPARISON WITH EXPERIMENT

To verify the hydrodynamic coefficients, the water tank experimental is carried out and the experiment conditions were as follows: The length of the water tank is 280 m, the beam is 10 m, and the depth is 10 m. Fig. 6 shows the water tank and the trimaran in the water tank.

FIGURE 6. (a) The trimaran in the water tank, (b) The water tank.

The wave spectrum adopts ITTC two-parameter spectrum above, $W2F$ and $W2M$ can be obtained by parameter identification. According to the above Fig. 6, the heave pitch values under different sea conditions and functions can be obtained. We give the conditions of 40 knots, SSN4 as an example, and the heave and pitch of the trimaran are obtained, as shown in Fig. 7.

According to Fig. 7, it shows that the hydrodynamic coefficients solved, based on CFD, is basically consistent with the experiment. This can be used as the simulation study for the subsequent controller design.

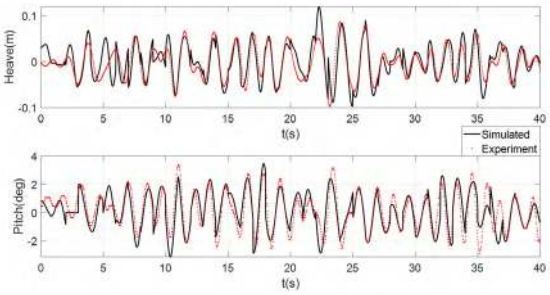

FIGURE 7. CFD simulation of the vertical motions and experimental comparison.

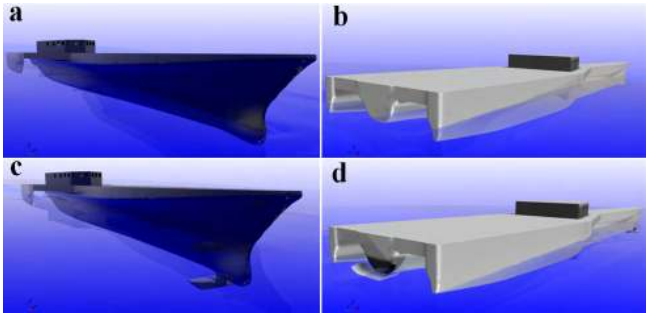

FIGURE 10. The trimaran with the fixed actuator (c and d) and no actuator (a and b) sailing in the heading wave.

III. STABILIZATION APPENDAGES

The actuators are T-foil and flap, hydraulic propulsion systems, and circuit systems. Through chapter 2, wave force and moment are obtained in different sea states, based on the wave force and moment, the sizes of T-foil and flap are designed, and the position of T-foil and flap installed on the trimaran is established. One T-foil was installed at the bow of the trimaran and a flap was installed at the rear. The airfoil of the T-foil is NACA0012 [30], the three-dimensional view and the size of both the T-foil and flap are shown in Fig. 8.

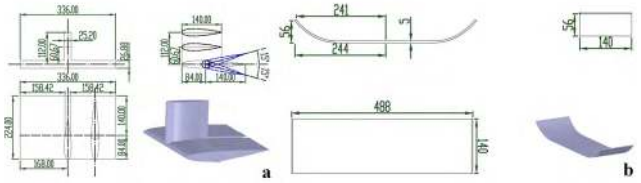

FIGURE 8. Sizes and 3D model of T-foil (a) and flap (b).

A. INSTALLATION POSITION OF ACTUATORS ON THE TRIMARAN

The T-foil and flap were installed into the trimaran as shown in Fig. 9 to verify the effect of trimaran vertical stabilization.

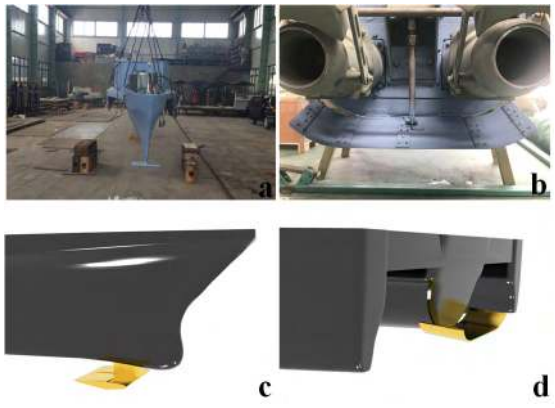

FIGURE 9. Installation of T-foil (a and c) and flap (b and d) on the trimaran.

The longitudinal distance is 420 mm from the centerline of the pillar to the bow (20 stations), and the vertical distance is 61 mm from the string line of the horizontal wing section to the trimaran baseline. The above model is compared with the naked trimaran for simulation, as shown in Fig. 10.

The experimental conditions are: the trimaran's speeds are 18 knots and 40 knots, and the sea states are SSN3 and SSN4. The following is an analysis of the results of trimaran vertical stabilization. However, for irregular waves, an accurate trimaran vertical stabilization effect can't be obtained by direct observation. Therefore, the method of judging wave height is used to estimate heave and pitch. First, heave and pitch are rendered as wave shapes and we mark the trough and crest, then the height is obtained by subtracting the crest from the trough. Finally, the height is ranked, and the first third of height from the largest to the smallest is selected as the sense data. An example of heave data at 40 knots SSN4 is selected and the result is shown in Fig.11.

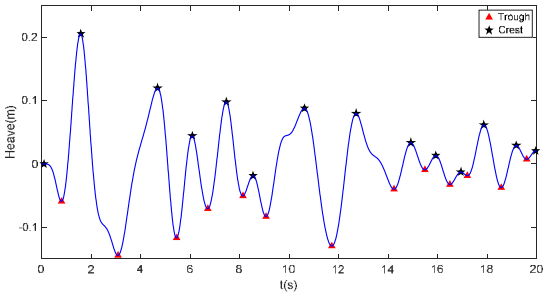

FIGURE 11. Trough and Crest mark.

According to the above method, the vertical stabilization situation of a trimaran equipped with a fixed actuator can be obtained, Table 4 proves that the designed and installed T-foil and flap have an obvious vertical stabilization effect. To achieve a better stabilization effect, a control system is designed for actuators and the force at a different speed and attack angle of the T-foil and flap must be calculated.

B. T-FOIL AND FLAP LIFT FORCE

For the design of the controller, it is important to know how much lift can be provided by the T-foil and flap.

TABLE 4. Simulation of the trimaran with the fixed actuator and no actuator at different sea states and speeds.

Speed/Sea condition	Heave	Pitch
18 knots/SSN3	14.18%	13.49%
18 knots/SSN4	7.29%	10.22%
40 knots/SSN3	25.61%	30.45%
40 knots/SSN4	16.07%	23.49%

Here, the CFD method is still used to calculate the lift force that is provided by the T-foil and flap.

The lift force, generated by different attack angles, is calculated separately, six attack angles of the T-foil and flap are calculated, the range of the T-foil and flap are $15^\circ \sim 15^\circ$ and $-7.5^\circ \sim 7.5^\circ$. As the airfoil is NACA 0012, it is a symmetry airfoil. Thus, the lift force at 0° is considered to be 0 N.

After calculation, we can obtain the lift force of the T-foil and flap at 18 knots and 40 knots. These results are shown in Table 5.

TABLE 5. The force of the T-foil and flap at different speeds and attack angles.

T-foil (deg)	T-40 knots (N)	T-18 knots (N)	Flap (deg)	F-40 knots (N)	F-18 knots (N)
-15°	-772.05	-144.46	-7.5°	-492.56	-125.64
-10°	-460.65	-82.25	-5°	-374.78	-79.92
-5°	-211.28	-26.50	-2.5°	-201.95	-39.93
5°	267.65	63.31	2.5°	202.45	41.06
10°	532.11	121.01	5°	454.19	98.63
15°	847.06	181.09	7.5°	679.19	146.95

The reason the T-foil and flap have vertical stabilization properties is that the force and moment provided by the actuators can inhibit the wave force and moment. The equation for the lift force and moment of the T-foil is as follows [31].

$$F_T = \frac{1}{2}\rho A U^2 C_L \theta \tag{15}$$

$$M_T = F_T l \tag{16}$$

where ρ is the seawater density, A is the area of T-foil, U is the speed of the trimaran, C_L is the lift coefficient, θ is the attack angle, and l is the distance between the center of the actuators and the center of the trimaran.

For the controller design, to control the attack angle of the T-foil and flap, it is needed to change the lift force and moment provided by the T-foil and flap. For this purpose, the slope of the lift force curve is needed for the calculation and we can directly obtain the relationship between the lift force and attack angle. The above Eq. (15) and Eq. (16) can be rewritten as:

$$F_T = \frac{1}{2}\rho A U^2 C_L \theta_1 = k_1 \theta_1 \tag{17}$$

$$M_T = F_T l_1 = k_1 l_1 \theta_1 \tag{18}$$

$$F_F = k_2 \theta_2 \tag{19}$$

$$M_F = k_2 l_2 \theta_2 \tag{20}$$

where l_1, l_2 are the distances of T-foil and flap relative to the center of the trimaran, k_1 and k_2 are the T-foil and flap lift force slopes, F_T, M_T, F_F, and M_F are the T-foil force and moment, flap force and moment, respectively. In [32] and [33], the T-foil's maximum angle is $\pm 15^\circ$ and the flap's angle is $0^\circ - 15^\circ$. The flap is usually in the medial position of the range, and the maximum angle is equivalent to $\pm 7.5^\circ$. Through approximate fitting, we can obtain the slope of the lift force on the T-foil and flap with different attack angles, Fig. 12 and Fig. 13 show the polynomial fitting at 40 knots and 18 knots, respectively.

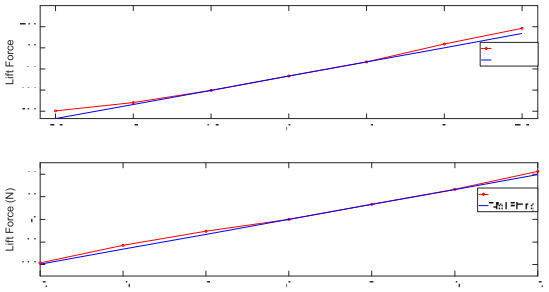

FIGURE 12. The fitting of T-foil and flap force at 40 knots.

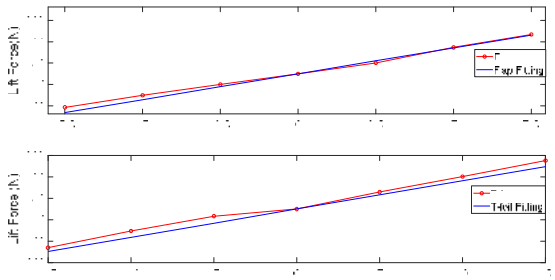

FIGURE 13. The fitting of T-foil and flap force at 18 knots.

From the above, the lift force of the T-foil and flap, at different speeds is much higher than the resistance. Therefore, the drag force can be ignored and approximately solved. The lift forces of the T-foil at 40 knots and 18 knots are 53.8 and 10.63, the slope of the lift forces the flap at 40 knots and 18 knots are 80.6 and 19.34, respectively.

IV. CONTROL SYSTEM DESIGN

A. THE ANALYSIS METHOD OF T-FOIL AND FLAP DECOUPLING

The trimaran motion equations with T-foil and flap can be rewritten as:

$$(m + a_{33})\ddot{x}_3 + b_{33}\dot{x}_3 + c_{33}x_3 + a_{35}\ddot{x}_5 + b_{35}\dot{x}_5 + c_{35}x_5 = F_r \tag{21}$$

$$(I_{yy}+a_{55})\ddot{x}_5+b_{55}\dot{x}_5+c_{55}x_5+a_{53}\ddot{x}_3+b_{53}\dot{x}_3+c_{53}x_3=M_r \tag{22}$$

where, $F_r = F_5 - F_T - F_F, M_r = M_5 - M_T - M_F$ For the trimaran vertical stabilization controller, the first step is to determine the correct logic relation between the trimaran motion trend and the actuator's attack angle trend. The heave motion of the trimaran is "+" when it is upward and "−" when it is downward. The pitch motion when the bow is upward and the stern is downward is "+" and when the bow is downward and the stern is upward is "−". Therefore, the force direction of the T-foil and flap during the trimaran movement is shown in Fig. 14.

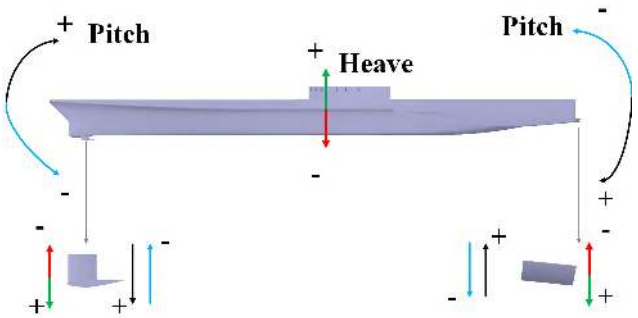

FIGURE 14. The change logic diagram of the attack angle of the actuator.

In Fig. 14, when the heave motion of the trimaran is upward, the T-foil and flap need to provide a downward force at the same time. Therefore, the T-foil and flap should simultaneously change their attack angles. When the prow of a trimaran points upward and the stern points downward, the T-foil is required to provide a downward force and the flap is required to provide an upward force. In this case, the T-foil should be applied at an upward attack angle and the flap at a downward attack angle. Therefore, there is a coupling relationship between the T-foil and Flap, and an incorrect control strategy will lead to boost-up the heave and pitch. In the process of the controller design, first of all, decoupling the T-foil and flap are necessary, then the controller is designed after the logical relationship is determined. The control system with the decoupling block diagram of the trimaran is described in Fig. 15:

In the analysis above, a PD controller based on the decoupling is designed. The control objective is to make the heave and pitch motions of the trimaran approach to 0 through the controller to control the attack angle of the T-foil and flap. Since there is a certain coupling relationship between T-foil and flap, it will increase heave and pitch motions by the incorrect decoupling method, so the correct decoupling must be considered when designing it. According to the literature [10], the decoupling filter can be written as follows:

$$w = \begin{pmatrix} 1 & w_2 \\ w_3 & 1 \end{pmatrix} \tag{23}$$

Based on the trimaran mathematical equation, the following equation is obtained:

$$w_2 = \frac{a_{w1}s^2 + a_{w2}s + a_{w3}}{b_{w1}s^2 + b_{w2}s + b_{w3}} \tag{24}$$

$$w_3 = \frac{a_{x1}s^2 + a_{x2}s + a_{x3}}{b_{x1}s^2 + b_{x2}s + b_{x3}} \tag{25}$$

where a_{wi} and a_{xi} $(i = 1, 2, 3)$ can be obtained according to the numerator and denominator of the coefficients of the trimaran equation. Using the method above in experimental test, the results of the controller is shown as follows:

TABLE 6. The effect of the decoupling stabilization controller.

Speed/SSN	Heave	Pitch
18knots/SSN3	35.13%	48.25%
18knots/SSN4	27.63%	36.41%
40knots/SSN3	32.47%	41.04%
40knots/SSN4	29.32%	38.65%

According to Table 6, it can be obtained the effectiveness of the decoupling algorithm for the trimaran vertical stabilization. Define C_1, U_1 as the input and output, before and after the decoupling link of heave loop, C_2, U_2 are the input and output, before and after the decoupling link of the pitch loop, in this condition,$C_1 = \theta_1$, $C_2 = \theta_2$, $U_1 = u_1$ and $U_2 = u_2$, then w_2 and w_3 can be rewritten as:

$$w_2 = \frac{a_{w1}s^2 + a_{w2}s + a_{w3}}{b_{w1}s^2 + b_{w2}s + bw_3} = \frac{C_1 - U_1}{U_2} \tag{26}$$

$$w_3 = \frac{a_{x1}s^2 + a_{x2}s + a_{x3}}{b_{x1}s^2 + b_{x2}s + b_{x3}} = \frac{C_2 - U_2}{U_1} \tag{27}$$

Take the sampling time $T = 0.02s$, we simplify and transform the above Eq. (26) and Eq. (27) and write it as a difference equation:

$$\begin{aligned} C_1(k) = {} & \frac{a_{m1}/T^2 + a_{m2}/T + a_{m3}}{b_{m1}/T^2 + b_{m2}/T + b_{m3}}U_2(k) \\ & - \frac{2a_{m1}/T^2 + a_{m2}/T}{b_{m1}/T^2 + b_{m2}/T + b_{m3}}U_2(k-1) \\ & + \frac{a_{m1}/T^2}{b_{m1}/T^2 + b_{m2}/T + b_{m3}}U_2(k-2) \\ & + U_1(k) - \frac{2b_{m1}/T^2 + b_{m2}/T}{b_{m1}/T^2 + b_{m2}/T + b_{m3}}U_1(k-1) \\ & + \frac{b_{m1}/T^2}{b_{m1}/T^2 + b_{m2}/T + b_{m3}}U_1(k-2) \\ & + \frac{2b_{m1}/T^2 + b_{m2}/T}{b_{m1}/T^2 + b_{m2}/T + b_{m3}}C_1(k-1) \\ & - \frac{b_{m1}/T^2}{b_{m1}/T^2 + b_{m2}/T + b_{m3}}C_1(k-2) \\ C_2(k) = {} & \frac{a_{n1}/T^2 + a_{n2}/T + a_{n3}}{b_{n1}/T^2 + b_{n2}/T + b_{n3}}U_1(k) \end{aligned} \tag{28}$$

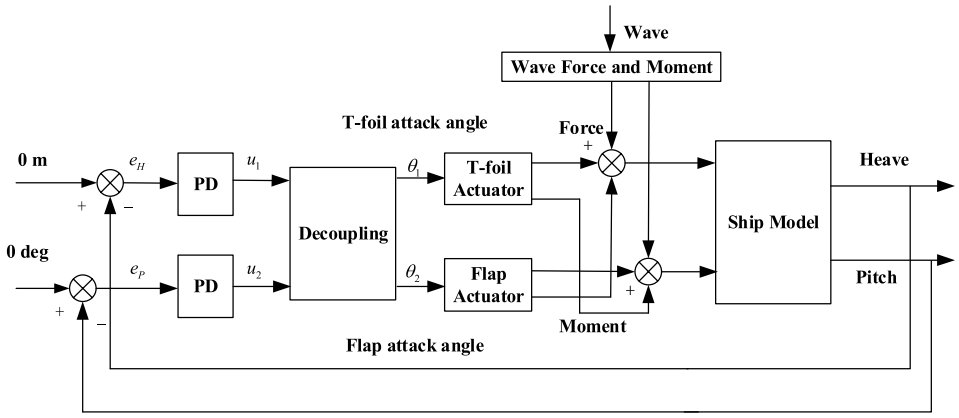

FIGURE 15. Trimaran control system with decoupling filter.

$$
\begin{aligned}
&- \frac{2a_{n1}/T^2 + a_{n2}/T}{b_{n1}/T^2 + b_{n2}/T + b_{n3}} U_1(k-1) \\
&+ \frac{a_{n1}/T^2}{b_{n1}/T^2 + b_{n2}/T + b_{n3}} U_1(k-2) \\
&+ U_2(k) - \frac{2b_{n1}/T^2 + b_{n2}/T}{b_{n1}/T^2 + b_{n2}/T + b_{n3}} U_2(k-1) \\
&+ \frac{b_{n1}/T^2}{b_{n1}/T^2 + b_{n2}/T + b_{n3}} U_2(k-2) \\
&+ \frac{2b_{n1}/T^2 + b_{n2}/T}{b_{n1}/T^2 + b_{n2}/T + b_{n3}} C_2(k-1) \\
&- \frac{b_{n1}/T^2}{b_{n1}/T^2 + b_{n2}/T + b_{n3}} C_2(k-2) \qquad (29)
\end{aligned}
$$

where the coefficients are obtained from the trimaran equation.

From the above equations, the order of the system is rather high, and in practical applications, it is difficult to implement because of the following remark

Remark 1: There are glitches in the heave and pitch data, the second-order difference can make these glitches larger.

Remark 2: The decoupling method above needs an accurate ship movement equation, errors exist in the process of the calculation and the decoupling equations maybe not accurate, the controller effect is weakened.

So, the idea of the decoupling above is good, but there may exist some problems, to avoid those problems of remark 1 and remark 2, the resultant force and moment distribution for dynamic decoupling is presented in the following part.

B. RESULTANT FORCE AND MOMENT DISTRIBUTION

The heave and pitch motions of the trimaran are mainly caused by the wave force and moment. The controller is designed to control the attack angle of the actuator to inhibit the wave force and moment as much as possible. Eq. (7) shows that both wave force and moment can generate heave and pitch, which means that both the T-foil and flap have an impact on heave and pitch. Thus, the control input of T-foil and flap need to be decoupled. According to Fig. 23,

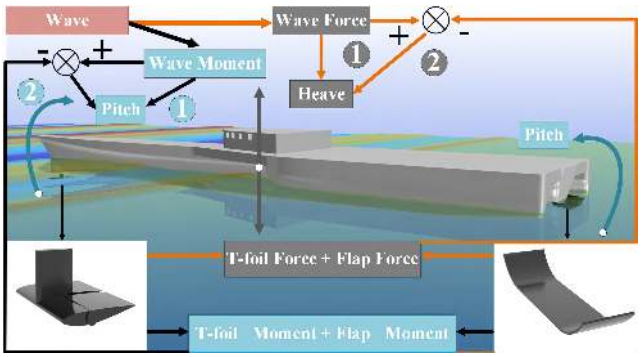

FIGURE 16. Resultant force and moment distribution.

the direction of the force is consistent with the heave direction, and the direction of the moment is consistent with the pitching direction. Therefore, it is considered that the force mainly produces heave motion, and the moment produces pitch motion. Fig. 16 shows the relationship of the resultant force and moment of the T-foil and flap to inhibit wave force and moment.

In Fig. 16, the trimaran movement is divided into two stages. The first stage is the wave force and moment on the trimaran. The second stage is the actuators force and moment inhibiting wave force and the moment, then the remaining force and the moment on the trimaran.

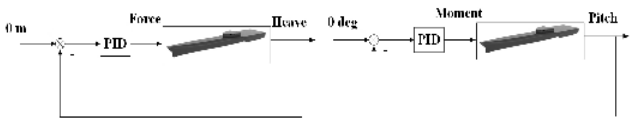

FIGURE 17. Heave-Force and Pitch-Moment.

By designing a controller based on the resultant force and moment distribution, the coupling control system shown in Fig. 16 can be separated into two separate control loops, as shown in Fig. 17. It has two controllers to control heave

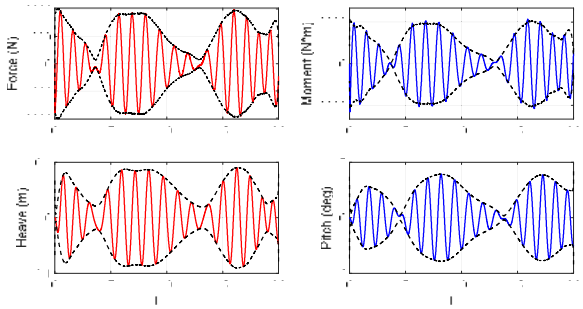

FIGURE 18. The envelop curve of heave, pitch, force, and moment.

and pitch, respectively. So, it can be considered a full actuated system [34].

Using the idea of the resultant force and moment distribution, the attack angles of the actuators are calculated in real-time. The wave force and moment on trimaran are F and M, the T-foil and flap forces are f_1 and f_2, and the distances from the T-foil and flap to the trimaran's center are l_1 and l_2, respectively. The idea is to use the resultant force of the T-foil and flap to offset the wave force as much as possible and also to use the resultant moment of the T-foil and flap to offset is the wave moment as much as possible. Therefore, the relationship between the resultant force and moment are defined as follows:

$$F = f_1 + f_2 \tag{30}$$
$$M = f_1 l_1 + f_2 l_2 \tag{31}$$

where F and M are based on the heave and pitch according to the decoupling of Chapter of 4.1. Through the simulation of 40 knots SSN4, the envelop curves of the heave, pitch, force and moment are shown in Fig. 18.

The force, heave, moment and pitch are all large. From the simulation data, the range of the force and heave are $-1915.9 \sim 1986.1$ N and $-0.0878 \sim 0.0903$ m, and the range of the moment and pitch are $-3254.4 \sim 3012.8$ Nm and $-3.9164 \sim 3.8137$ deg, respectively. Therefore, the relationship can be approximated by the maximum force based on maximum heave and the maximum moment based on maximum pitch, we take 22000 and 1000 for the force to heave and moment to pitch, and the according to amplitude it is as follows:

$$F = k_h \times Heave \tag{32}$$
$$M = k_p \times Pitch \tag{33}$$

By changing the above Eq. (30) and Eq. (31), the following equations can be obtained:

$$f_1 = (M - Fl_2)/(l_1 - l_2) \tag{34}$$
$$f_2 = (Fl_1 - M)/(l_1 - l_2) \tag{35}$$

According to Fig. 12 and Fig. 13, the relationship between the attack angle and the lift force of a trimaran at the speed of 40 knots and 18 knots are obtained by the fitting. Through Eq. (15), the slope of the fitting is calculated and it can be written as follows:

$$F_T = f_1 = k_1\theta_1 \tag{36}$$
$$M_T = f_1 l_1 = k_1 l_1 \theta_1 \tag{37}$$
$$F_F = f_2 = k_2\theta_2 \tag{38}$$
$$M_F = f_2 l_2 = k_2 l_2 \theta_2 \tag{39}$$

Based on the above Eq. (36)-(39), the attack angle can be calculated as follows:

$$\theta_1 = f_1/k_1 = (M - Fl_2)/k_1(l_1 - l_2) \tag{40}$$
$$\theta_2 = f_2/k_2 = (Fl_1 - M)/k_2(l_1 - l_2) \tag{41}$$

Then, the trimaran vertical stabilization control system based on the resultant force and moment distribution is shown in Fig. 19.

The dynamic decoupling method is presented and then the PD controller is designed. In this paper, the simulation and experimental analysis will be carried out through the idea of a sigmoid function PD controller and the method of the resultant force and moment distribution. Generally speaking, the idea of the sigmoid function is that the smooth curve can be distributed into countless tiny line segments with the length approaching 0, that is, the curve can be regarded as a broken line connected by an infinite number of tiny line segments. In this paper, a broken line connected by the values on the main diagonal of the rule table in a conventional fuzzy controller can be fitted with a sigmoid curve function [35], as follows:

$$y = 2.0/(1.0 + \exp(-kx)) - 1.0 \tag{42}$$

The characteristics of the sigmoid function are shown in Fig. 20.

The controller designed with the sigmoid function is called the S-plane PD controller, and its control law is shown as follows:

$$u = 2.0/(1.0 + \exp(-k_p e - k_d \dot{e})) - 1.0 \tag{43}$$

where u is the control input of the controlled objective, k_p, k_d are parameters of the controller,e and $\dot{e}$ are the deviation of the controlled quantity and the change rate of the deviation, respectively.

In Fig. 20, the changes in the controller parameter k causes the sigmoid function curve to change. The larger the value of k, the larger the output of the controller will be under the same input condition and the control degree will be enhanced. In the sigmoid function curve with a constant k value, the smaller the absolute value of controller input, the smaller its control output is. In the control theory, the S-plane control can be regarded as a simple fuzzy controller with the idea of fuzzy control [36]. Because of its convenient design and obvious control effect, this paper adds the idea of S-plane controlled into the controller. The direct outputs of the S-plane controller are ΔF and ΔM. It can be understood, that the larger e, the greater the control effect of the S-plane

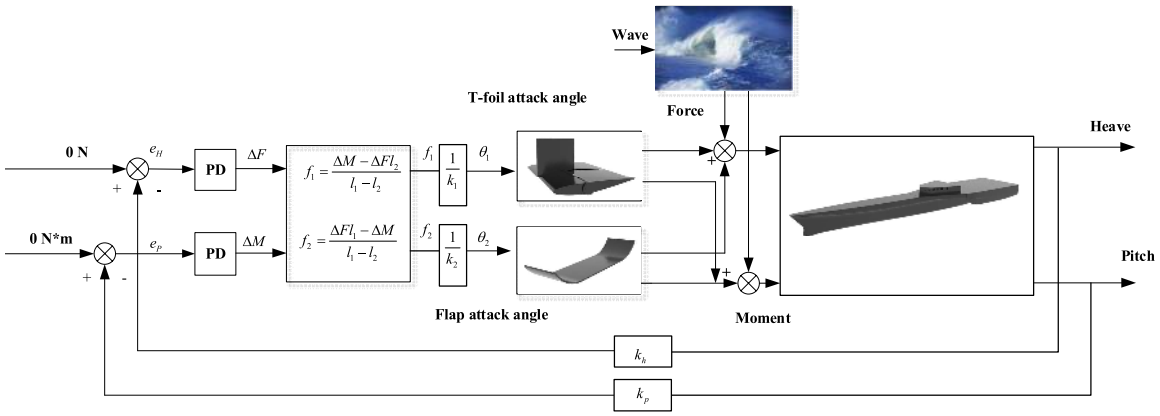

FIGURE 19. Trimaran control system based on resultant force and moment distribution.

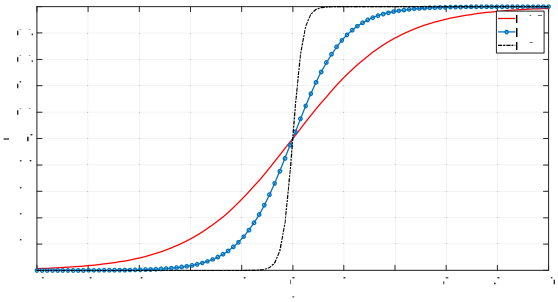

FIGURE 20. Different parameters of the s-plane PD's effect on the control effect.

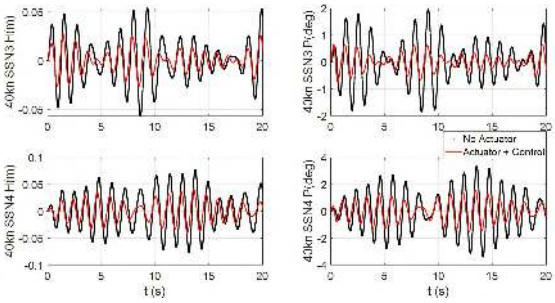

FIGURE 21. Comparison of S-plane resultant force and moment PD controlled actuator with no actuator in simulation.

PD controller on the target is, and the larger ΔF and ΔM are. In Eq. (32) and Eq. (33), the amplitude of the biggest force to heave and moment to pitch are presented, k_{h} and k_p represent the corresponding relations, then using these the control law is shown as follows:

$$u_1 = 2.0/(1.0 + \exp(-k_{hp}e - k_{hd}\dot{e})) - 1.0 \quad (44)$$

$$u_2 = 2.0/(1.0 + \exp(-k_{pp}e - k_{pd}\dot{e})) - 1.0 \quad (45)$$

$$\Delta F = k_{\mathrm{h}} \times u_1 \quad (46)$$

$$\Delta M = k_p \times u_2 \quad (47)$$

where $k_{hp}, k_{hd}, k_{pp}, k_{pd}$ are the controller parameters, and $-1 \leq u_1 \leq 1, -1 \leq u_2 \leq 1$.

The simulation analysis was carried out and the numerical values of heave and pitch of the trimaran were obtained through CFD analysis, taking the SSN4 of uniform scaling and 40 knots speed as examples. The values of k_{h} and k_p are 22000 and 1000, respectively. Through multiple simulations and finding the appropriate parameters, adjusting the controller parameters k_{hp}, k_{hd}, k_{pp} and k_{pd}, to 30, 2, 3 and 3, respectively, and putting the above formula into the simulation environment, the effect of the resultant force and moment distribution is obtained as follows. The curve below shows the trimaran without actuators and active controlled actuators:

Judging from the above Fig. 21, the heave and pitch can be reduced by 52.60% and 62.29%, in the condition of 40 knots, and reduced 47.78% and 53.12%, in the condition of 40 knots SSN4, respectively, which proves the effectiveness of the resultant force distribution method. The following chapter uses the method of the resultant force and moment distribution combine with a PD controller based on the s-plane for experimental analysis.

V. EXPERIMENT ANALYSIS

The trimaran was towed in an experimental tank with active controlled T-foil and flap. The experiments were carried out at the same ratio of SSN3 (wave height and period were 0.1 m and 1.79 s) and SSN4 (wave height and period were 0.2 m and 2.12 s), with a speed of 6.5073 m/s and 2.93 m/s, respectively. Fig. 22 shows the experiment state.

The experiment of the trimaran with an actuator and active control is carried out, and it can be divided into four conditions including 18 knots SSN3, 18 knots SSN4, 40 knots SSN3 and 40 knots SSN4. Waves, heave, pitch, T-foil, and flap in four cases are given respectively, as shown in Fig. 23-Fig. 27. The length of the water tank is 280 m. We found a distance of around 160 m, which is the length of the water tank minus the distance of the trailer's acceleration and deceleration stage, to be stable. When the trimaran speed

FIGURE 22. (a) The trimaran with the actuator in the water tank; (b) trimaran with S-plane PD controller sailing in the water tank.

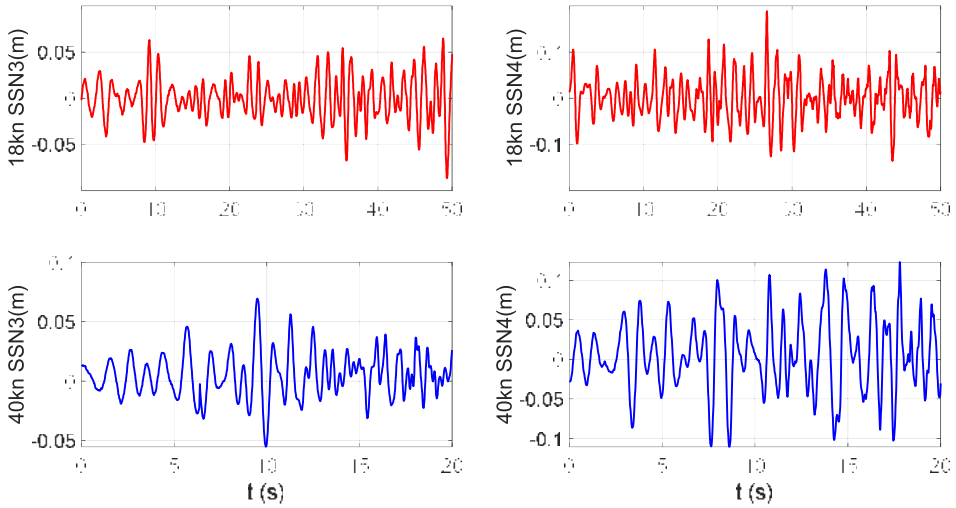

FIGURE 23. Wave height of different speeds and sea states.

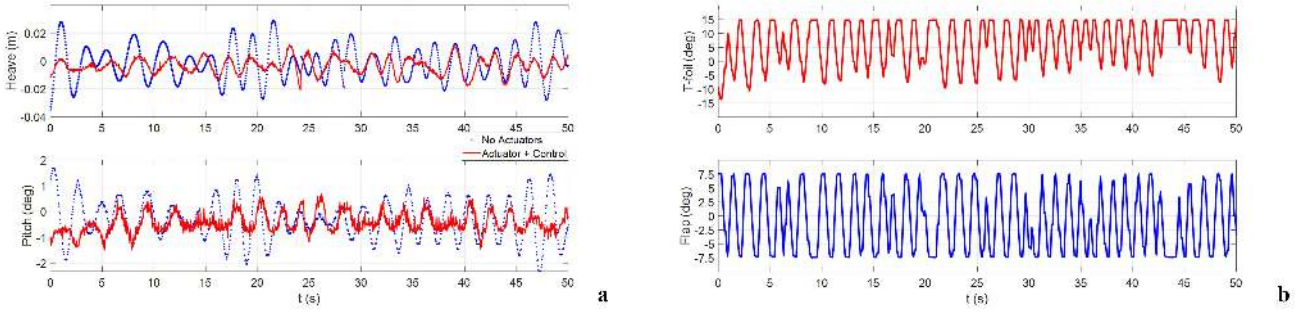

FIGURE 24. Comparison of active actuators controlled with no actuators on the trimaran in 18 knots SSN3 (a), T-foil and flap attack angle change at 18 knots, SSN3 (b).

is 18 knots, the effect time is 54.6 s, and in 40 knots the acceleration and deceleration time are longer, so the effective time at 40 knots is shorter. The effective time at 18 knots and 40 knots are 50 s and 20 s, respectively, and the sampling frequency is 50 HZ.

1). Wave in four experimental conditions:

2). Heave and pitch motions at 18 knots, SSN3 are shown in Fig. 24 below:

3). Heave and pitch motions at 18 knots, SSN4 are shown in Fig. 25 below:

4). Heave and pitch motions at 40 knots, SSN3 are shown in Fig. 26 below:

5). Heave and pitch motions at 40 knots, SSN4 are shown in Fig. 27 below:

From the four conditions above, the vertical stabilization effect is obtained in Table 7.

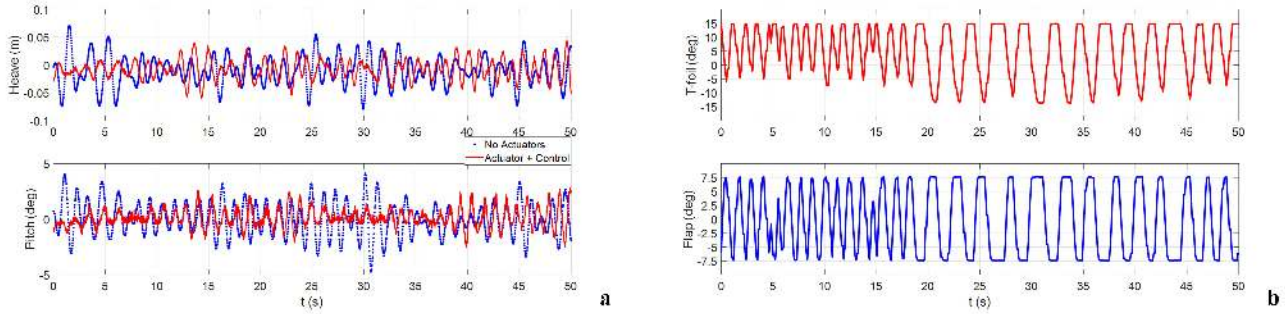

FIGURE 25. Comparison of active actuators controlled with no actuators on the trimaran in 18 knots SSN4 (a), T-foil and flap attack angle change at 18 knots, SSN4 (b).

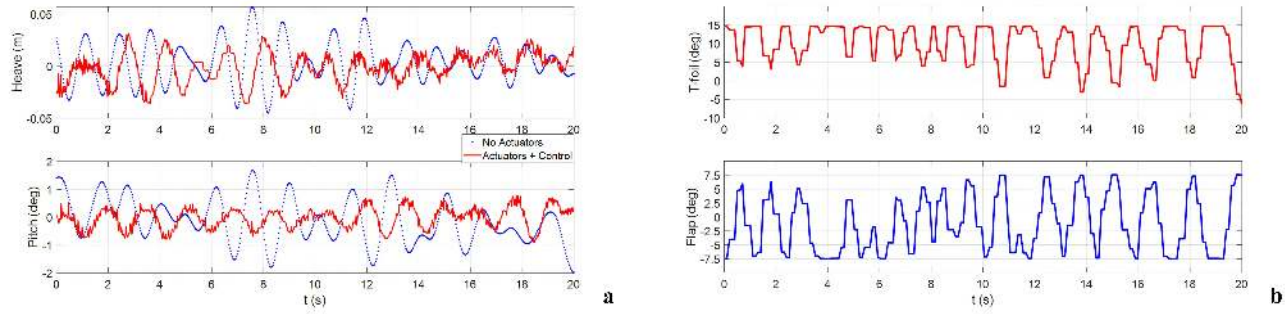

FIGURE 26. Comparison of active actuators controlled with no actuators on the trimaran in 40knots SSN3 (a), T-foil and flap attack angle change at 40 knots, SSN3 (b).

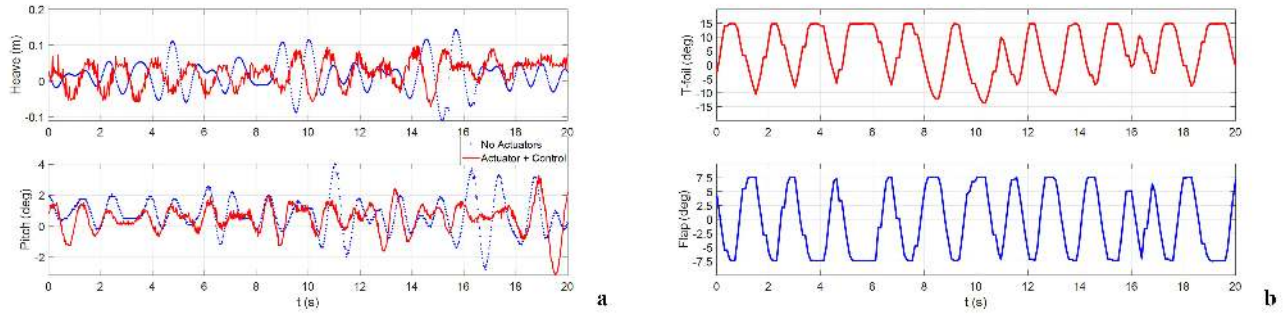

FIGURE 27. Comparison of active actuators controlled with no actuators on the trimaran in 40knots SSN4 (a), T-foil and flap attack angle change at 40 knots, SSN4 (b).

TABLE 7. The experimental results of the trimaran with a PD controlled actuator and no actuator at different sea states and speeds.

Speed/Sea condition	Heave	Pitch
18 knots/SSN3	46.69%	57.52%
18 knots/SSN4	37.20%	41.03%
40 knots/SSN3	36.37%	58.79%
40 knots/SSN4	31.31%	40.67%

VI. CONCLUSIONS

This work describes research on reducing the heave and pitch motions on a trimaran, T-foil and flap with an active control are used, CFD with the mathematical model is developed to facilitate control studies, and CFD results were carried out on an experimental basis.

The effect of this research is shown in Table 6, it can be further by improving the size of actuators, the control method, and parameters. The size of the actuators needs to be optimal. When increasing the area of the actuator, the force and moment provided by the actuator are increased, but the trimaran's resistance is also increased and the optimal point should be considered. After that, an advanced control algorithm should be applied to trimaran vertical stabilization, and this will improve the vertical stabilization effect.

The trailer towing the trimaran leads to the trimaran's bow being raised. So, the T-foil attack angle has an upward trend and its influence increases as the speed increases, it reduces the vertical stabilization effect. Also, as the trailer

speed increased, the upward trend increased. So, in the water tank, the trimaran vertical stabilization effect was influenced. Future work will research the MSI of the trimaran and optimal configurations for the actuators and controller to improve the vertical stabilization effect.

REFERENCES

[1] C.-C. Fang and H.-S. Chan, "An investigation on the vertical motion sickness characteristics of a high-speed catamaran ferry," *Ocean Eng.*, vol. 34, nos. 14–15, pp. 1909–1917, 2007.

[2] C. Hong and Y. X. Chen, "Current situation and tendency of development of ship stabilizer technique," *Ship Eng.*, vol. 34, no. S2, pp. 236–244, 2012.

[3] W. Liu, Y. K. Demirel, and E. B. Djatmiko, "Bilge keel design for the traditional fishing boats of Indonesia's East Java," *Int. J. Nav. Archit. Ocean Eng.*, vol. 11, no. 1, pp. 380–395, 2019.

[4] M. T. Sharif, G. N. Roberts, and R. Sutton, "Final experimental results of full scale fin/rudder roll stabilisation sea trials," *Control Eng. Pract.*, vol. 4, no. 3, pp. 377–384, 1996.

[5] J. AlaviMehr, J. Lavroff, M. R. Davis, D. S. Holloway, and G. A. Thomas, "An experimental investigation of ride control algorithms for high-speed catamarans Part 1: Reduction of ship motions," *J. Ship Res.*, vol. 61, no. 1, pp. 35–49, 2017.

[6] L. H. Liang, M. X. Sun, S. T. Zhang, Y. Wen, and Y. W. Liu, "A integrate control system design of WPC with active T-foil and transom stern flap for vertical motion improvement," *J. Comput. Inf. Syst.*, vol. 11, no. 9, pp. 3217–3227, 2015.

[7] Z. Zong, Y. Sun, and Y. Jiang, "Experimental study of controlled T-foil for vertical acceleration reduction of a trimaran," *J. Mar. Sci. Technol.*, vol. 24, no. 2, pp. 553–564, 2019.

[8] J. Aranda, J. M. de la Cruz, and J. M. Diaz, "Design of a multivariable robust controller to decrease the motion sickness incidence in fast ferries," *Control Eng. Pract.*, vol. 13, no. 8, pp. 985–999, 2005.

[9] M. Santos, R. López, and J. M. de la Cruz, "Fuzzy control of the vertical acceleration of fast ferries," *Control Eng. Pract.*, vol. 13, no. 3, pp. 305–313, 2005.

[10] J. M. de la Cruz, J. Aranda, J. M. Giron-Sierra, F. Velasco, S. Esteban, J. M. Diaz, and B. de Andres-Toro, "Improving the comfort of a fast ferry," *IEEE Control Syst.*, vol. 24, no. 2, pp. 47–60, Apr. 2004.

[11] S. Esteban, J. M. Giron-Sierra, B. De Andres-Toro, J. M. de la Cruz, and J. M. Riola, "Fast ships models for seakeeping improvement studies using flaps and T-foil," *Math. Comput. Model.*, vol. 41, no. 1, pp. 1–24, 2005.

[12] J. Arandam J. M. Díaz, P. Ruipérez, T. M. Rueda, and E. López, "Decreasing of the motion sickness incidence by a multivariable classic control for a high speed ferry," *IFAC Proc. Volumes*, vol. 34, no. 7, pp. 273–278, 2001.

[13] M.-C. Fang and J.-H. Luo, "On the track keeping and roll reduction of the ship in random waves using different sliding mode controllers," *Ocean Eng.*, vol. 34, nos. 3–4, pp. 479–488, 2007.

[14] J. Liu, R. Allen, and H. Yi, "Ship motion stabilizing control using a combination of model predictive control and an adaptive input disturbance predictor," *Proc. Inst. Mech. Eng., I, J. Syst. Control Eng.*, vol. 225, no. 5, pp. 591–602, 2011.

[15] L. Liang, J. Yuan, S. Zhang, and P. Zhao, "Design a software real-time operation platform for wave piercing catamarans motion control using linear quadratic regulator based genetic algorithm," *PLoS ONE*, vol. 13, no. 4, 2018, Art. no. e0196107.

[16] M. Ertogan, S. Ertugrul, and M. Taylan, "Application of particle swarm optimized PDD^2 control for ship roll motion with active fins," *IEEE/ASME Trans. Mechatronics*, vol. 21, no. 2, pp. 1004–1014, Apr. 2016.

[17] W. Luo, B. Hu, and T. Li, "Neural network based fin control for ship roll stabilization with guaranteed robustness," *Neurocomputing*, vol. 230, pp. 210–218, Mar. 2017.

[18] T. Takami, S. Matsui, M. Oka, and K. Iijima, "A numerical simulation method for predicting global and local hydroelastic response of a ship based on CFD and FEA coupling," *Mar. Struct.*, vol. 59, pp. 368–386, May 2018.

[19] Y. Su, W. Shuo, H. Shen, and D. U. Xin, "Numerical and experimental analyses of hydrodynamic performance of a channel type planing trimaran," *J. Hydrodyn.*, vol. 26, no. 4, pp. 549–557, 2014.

[20] A. Fitriadhy, M. K. Aswad, N. A. Aldin, N. A. Mansor, A. A. Bakar, and W. B. Nik, "Computational fluid dynamics analysis on the course stability of a towed ship," *J. Mech. Eng. Sci.*, vol. 11, no. 3, pp. 2919–2929, 2017.

[21] S. S. Kianejad, H. Enshaei, J. Duffy, and N. Ansarifard, "Prediction of a ship roll added mass moment of inertia using numerical simulation," *Ocean Eng.*, vol. 173, pp. 77–89, Feb. 2019.

[22] J. Wang, L. Zou, and D. Wan, "Numerical simulations of zigzag maneuver of free running ship in waves by RANS-Overset grid method," *Ocean Eng.*, vol. 162, pp. 55–79, Aug. 2018.

[23] Z. Shen, D. Wan, and P. M. Carrica, "Dynamic overset grids in OpenFOAM with application to KCS self-propulsion and maneuvering," *Ocean Eng.*, vol. 108, pp. 287–306, Nov. 2015.

[24] R. Muñoz-Mansilla, J. Aranda, J. M. Díaz, D. Chaos, and J. M. de la Cruz, "Identification of longitudinal and transversal dynamics of a fast ferry," *IFAC Proc. Volumes*, vol. 41, no. 2, pp. 15967–15972, 2008.

[25] P. Tristan, *Ship Motion Control: Course Keeping and Roll Stabilisation Using Rudder and Fins*. London, U.K.: Springer, 2010, pp. 17–44.

[26] M.-C. Fang, Y.-H. Lin, and B.-J. Wang, "Applying the PD controller on the roll reduction and track keeping for the ship advancing in waves," *Ocean Eng.*, vol. 54, pp. 13–25, Nov. 2012.

[27] L. Moreira, T. I. Fossen, and C. G. Soares, "Path following control system for a tanker ship model," *Ocean Eng.*, vol. 34, nos. 14–15, pp. 2074–2085, 2007.

[28] R. Muñoz-Mansilla, J. Aranda, J. M. Díaz, and J. de la Cruz, "Parametric model identification of high-speed craft dynamics," *Ocean Eng.*, vol. 36, nos. 12–13, pp. 1025–1038, 2009.

[29] Y. Marinakis, M. Marinaki, and A. Migdalas, "A multi-adaptive particle swarm optimization for the vehicle routing problem with time windows," *Inf. Sci.*, vol. 481, pp. 311–329, May 2019.

[30] I. H. Abbott and A. E. von Doenhoff, *Theory of Wing Sections, Including a Summary of Airfoil Data*. North Chelmsford, MA, USA: Courier Corporation, 1959.

[31] E. V. Lewis, *Principles of Naval Architecture*, 2nd ed. Hoboken, NJ, USA: SNAME, 1988.

[32] T. Kawazoe, S. Nishikido, and Y. Wada, "Effect of fin area and control methods on reduction of roll motion with fin stabilizers," *Bull. MESJ*, vol. 22, no. 1, pp. 25–32, 1994.

[33] R. P. Dallinga, "Hydrodynamical aspects of the design of fin stabilizers," *Trans. RINA*, pp. 189–200, 1993.

[34] A. Müller and P. Maisser, "Generation and application of prestress in redundantly full-actuated parallel manipulators," *Multibody Syst. Dyn.*, vol. 18, no. 2, pp. 259–275, 2007.

[35] S. Jin, J. Bak, J. Kim, T. Seo, and H. S. Kim, "Switching PD-based sliding mode control for hovering of a tilting-thruster underwater robot," *PLoS ONE*, vol. 13, no. 3, 2018, Art. no. e0194427.

[36] S. Banerjee, S. S. Chaudhuri, and S. Roy, "Fuzzy logic and log-sigmoid function based vision enhancement of hazy images," in *Proc. SAI Intell. Syst. Conf.* Cham, Switzerland: Springer, 2018, pp. 447–462.

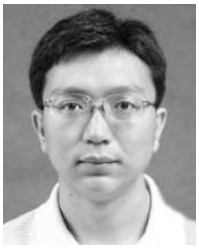

ZHILIN LIU was born in Harbin, China, in 1977. He received the B.A. degree in automatic control and the M.Sc. and Ph.D. degrees in control science and engineering from the Harbin Institute of Technology, in 2000, 2002, and 2007, respectively. In 2014, he was a Visiting Scholar with the Institute for Automatic Control and Complex Systems (AKS), University of Duisburg-Essen, Germany. He is currently an Associate Professor with the College of Automation, Harbin Engineering University. His research interests include model predictive control (MPC) and ship control.

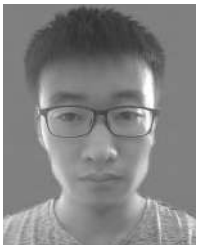

LINHE ZHENG was born in Suihua, China, in 1993. He is currently pursuing the Ph.D. degree with the College of Automation, Harbin Engineering University, China. His research interest includes ship motion stabilization control.

GUOSHENG LI was born in Yancheng, China, in 1992. He received the B.A. degree in automation and the M.Sc. degree in control science and engineering from Jiangsu University, Zhenjiang, China, in 2014 and 2017, respectively. He is currently pursuing the Ph.D. degree with the College of Automation, Harbin Engineering University, China. His research interests include ship motion control and model predictive control.

BOWEN ZENG was born in Changde, China, in 1976. He received the B.A. degree in industry automation, the M.Sc. degree in control science and engineering, and the Ph.D. degree in control science and engineering from Harbin Engineering University, in 2001, 2006, and 2012, respectively, where he is currently a Lecturer with the College of Automation. His research interests include ship motion control, and embedded system design and application.